

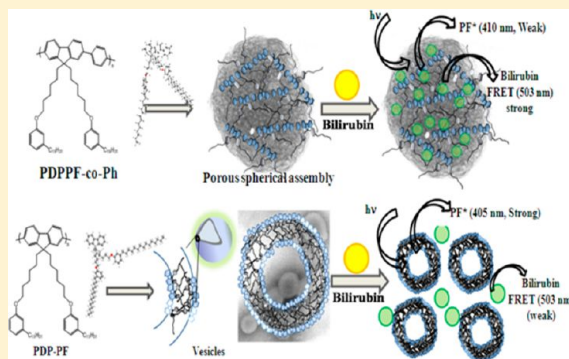
Self-Assembly in Tailor-Made Polyfluorenes: Synergistic Effect of Porous Spherical Morphology and FRET for Visual Sensing of Bilirubin

T. Senthilkumar and S. K. Asha*

Polymer & Advanced Material Laboratory, Polymer Science & Engineering Division, CSIR, NCL, Pune-411008, Maharashtra, India

Supporting Information

ABSTRACT: Two new fluorene-based homo- (PDP-PF) and copolymers (PDPPF-co-Ph) were synthesized with a bulky 3-pentadecylphenoxy (PDP) group appended hexyl chains at the 9, 9' position using Suzuki coupling polymerization. Investigation on the morphology of the polymers using microscopic techniques like TEM and AFM indicated formation of self-assembled nanostructures like vesicles by PDP-PF and porous spheres by PDPPF-co-Ph respectively. Dynamic as well as static light scattering studies (DLS, SLS) in THF also indicated the existence of self-assembled nanosized particles in solution with a shape factor (ρ) of 0.76 and 0.96 for PDP-PF and PDPPF-co-Ph, respectively, confirming the existence of vesicles in the case of the former and spherical particles in the case of the latter polymer. The favorable photophysical properties of the polyfluorenes were taken advantage of for the selective sensing of unbound bilirubin (BR) in THF. A high energy transfer efficiency of 86% upon addition of bilirubin with color change from blue (polyfluorene emission) to green (FRET-induced bilirubin emission) was observed with PDPPF-co-Ph. Steady state fluorescence measurements gave a minimum donor-acceptor distance of 36 Å and time-resolved fluorescence decay measurements showed a reduction in average lifetime of PDPPF-co-Ph (from 450 to 240 ps) upon addition of bilirubin indicating efficient energy transfer. The open porous spherical assembly of PDPPF-co-Ph enabled better adsorption of the analyte, which along with the good spectral overlap resulted in greater efficiency for FRET-induced energy transfer. Sensing of unbound bilirubin was also attempted in THF/water solvent mixture in an effort to simulate the unbound (THF soluble) and bound (water-soluble) bilirubin equilibrium. Enhancement of bilirubin emission coupled with quenching of polyfluorene emission makes this approach adaptable for visual fluorimetric color change (blue to green) based sensor. Structural analogues such as biliverdin and porphyrin showed poor fluorescence quenching efficiency, thus highlighting the selectivity and sensitivity of the FRET-based sensing of bilirubin by the newly designed polyfluorene.



INTRODUCTION

Conjugated polymers provide a good platform for a wide variety of applications such as light emitting diodes,¹ polymer solar cells,^{2,3} field effect transistors⁴ and sensors.^{5–8} The delocalized π electrons in these semiconductors are sensitive even to minor perturbations resulting in amplified signal response due to which they find applications as chemical and biosensors.⁹ The combination of amplified response and sensitivity in conjugated polymer-based sensors makes them superior compared to their small molecule counterparts.¹⁰ Generally, fluorescence-based sensors adopt three different strategies: (a) fluorescence quenching (turn-off), (b) fluorescence enhancement (turn-on), and (c) fluorescence resonance energy transfer (FRET). Bazan et al., developed a polyfluorene-based sensor that detected the hybridization of the single stranded deoxyribonucleic acid (ssDNA) with specific base sequence where the polyfluorene acted as the donor and dye labeled ssDNA acted as the acceptor.¹¹ FRET-induced energy transfer from the polymer to dye enhanced the emission of the dye compared to the direct excitation of the

dye. Another example of energy transfer based acceptor emission was demonstrated by Tapia et al., where energy transfer occurred from conjugated polyelectrolyte to meso-tetrakis-phenylporphyrinsulfonates resulting in decreased polymer emission, followed by a corresponding increase in the fluorescence of the porphyrin acceptors.¹² In the scenario of FRET-based enhanced acceptor emission, morphology of the donor polymer plays a major role as desirable morphologies like vesicles, porous assemblies, etc. enable close interaction of the donor and acceptor units.¹³ Vesicular morphology is very promising as drug delivery vehicles as they help encapsulate hydrophilic/hydrophobic drug molecules in their interior cavity depending on their structural constitution.¹⁴ In general, researchers have sought the help of amphiphilic (hydrophilic/hydrophobic combinations) structural modifications in polymers to explore self-assembled architectures like vesicles.¹⁵

Received: January 15, 2013

Revised: February 19, 2013

There have been reports where oligo/polyfluorenes modified with hydrophilic units have been used for sensing application based on the characteristic optical properties of the self-assembled nanoparticles.¹⁶ Reports on the application of conjugated homopolymers or conjugated polymers without the required amphiphilic structure for self-assembly for fluorescence-based sensing are very rare.

Here we report for the first time the sensing of bilirubin by conjugated polyfluorenes with high selectivity and sensitivity. Bilirubin is the breakdown product of hemoglobin and contains a tetrapyrrole moiety with six intramolecular hydrogen bonds existing in ridge tile conformation.¹⁷ Under normal physiological conditions bilirubin is mostly present as the conjugated form which is bound with human serum albumin (direct/bound bilirubin), which makes it water-soluble. The unconjugated or free fraction which is potentially toxic is usually present in small amounts and is excreted after enzymatically esterified with glucuronic acid.¹⁸ Abnormal levels of bilirubin – either conjugated or unconjugated, detected in serum samples is an indicator for disturbed bilirubin metabolism. For instance, increased levels of conjugated bilirubin in serum could signal disturbance of bile drainage as in obstructive jaundice or increased levels of unconjugated bilirubin could be due to abnormally high breakdown of hemoglobin (hemolysis).^{18,19} Therefore, monitoring the bilirubin concentration in body fluids is a vital step in diagnosing liver disorders and jaundice. Clinically, the levels of bilirubin (conjugated and unconjugated bilirubin) is determined by the color change from yellow to red produced by the diazotization reaction of bilirubin and sulphanic acid using spectrophotometer (total van den Bergh reaction, 1914).^{18,20} The major disadvantage of the assay is that it overestimates conjugated bilirubin and is time-consuming (30 min to develop the maximum color).²¹ There are only very few reports on fluorimetric bilirubin sensing; very recently a spectrofluorometric method of determination of free bilirubin by Kleinfeld et.al was described using mutated fatty acid binding protein labeled with the fluorescent molecule acrylodan or rhodamine-B, whose fluorescence changed upon binding to bilirubin.²² Till date there are no reports on bilirubin sensing using conjugated polymer as the fluorescent sensor. By taking advantage of overlapping photophysical properties of bilirubin and polyfluorenes we have developed a model polyfluorene sensor to detect unconjugated bilirubin via FRET process for the first time. Although simple dialkyl polyfluorenes like 9,9'-dioctylpolyfluorenes also exhibited complementary photophysical characteristics to bilirubin, its sensing efficiency was very low. In our molecular design we incorporated bulky pentadecyl phenol (PDP) units (which are well-known to have the ability to self-organize by way of alkyl chain interdigitation as well as aromatic π stacking interactions)²³ at the 9,9'-position of fluorene with the anticipation that the structurally modified polyfluorene would be able to self-assemble into desired morphologies resulting in close interaction with bilirubin. The self-assembled structures of the PDP substituted polyfluorenes were studied in solution state using static and dynamic light scattering (SLS and DLS), and in solid state using microscopic techniques like TEM and AFM. Steady states as well as time-resolved fluorescence analysis were conducted to study the donor–acceptor interaction parameters. An attempt was also made to sense the unbound bilirubin in presence of bound bilirubin by carrying out the fluorescence studies in THF/water (containing NaOH) media, where an equilibrium was created between the

water solvated (bound) bilirubin and organic media soluble (free) bilirubin. The selectivity and sensitivity of the bilirubin sensing by the new polyfluorene was verified with structurally analogous molecules like porphyrin which had very similar absorption spectra with that of bilirubin. The tailor-made polyfluorene structure presented here illustrates the importance of self-assembling building blocks like the PDP unit which helps induce self-organization even in the homopolymer, without having to design amphiphilic block copolymers or polymers incorporated with hydrophilic units like the oligooxyethylene to induce phase separation.

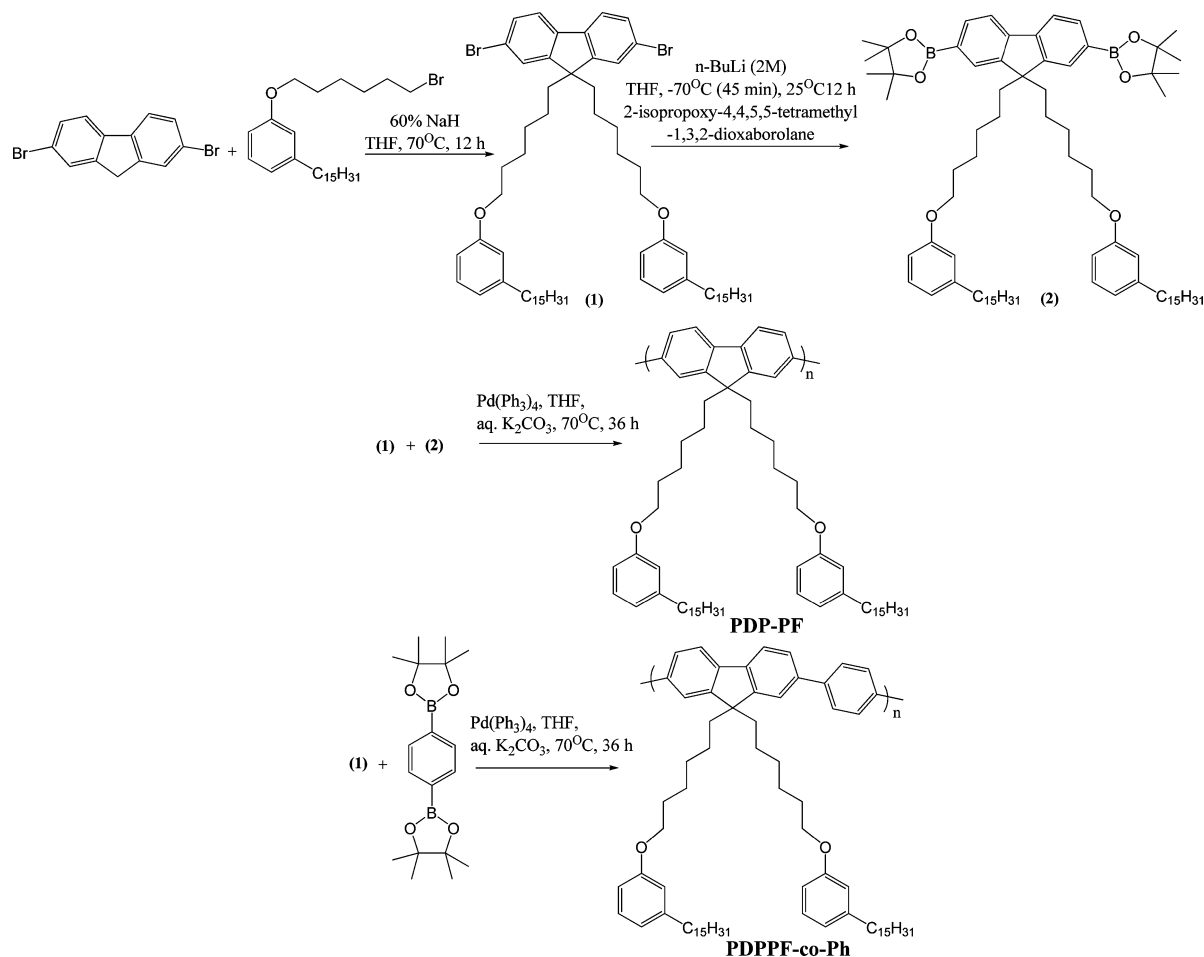
EXPERIMENTAL SECTION

Materials. 2,7-Dibromo-9H-fluorene, 3-pentadecylphenol, bilirubin, biliverdin, rhodamine, 5,10,15,20-tetrapyrrolyl-20H,25H-porphine, Pd(PPh₃)₄, 1,4-benzenediboronic acid, sodium hydride, 1,6-dibromohexane, 2-isopropoxy-4,4,5,5-tetramethyl-1,3,2-dioxaborolane, *t*-BuLi and 1-bromooctane were purchased from Aldrich Company Ltd. and were used as such. Potassium hydroxide, potassium carbonate and ethanol were purchased from Merck Chemicals Ltd. Tetrahydrofuran (THF), acetone and methanol were purchased locally and were purified using standard procedures.

Measurements. ¹H NMR was recorded on a Bruker-AVENS 200 MHz spectrometer. Chemical shifts are reported in ppm at 25 °C using CDCl₃ as solvent containing small amount of tetramethylsilane (TMS) as internal standard. The purity of the compounds was determined by elemental analysis as well as MALDI–TOF in combination with size exclusion chromatography (SEC). Elemental analysis was done by Thermofinnigan flash EA 1112 series CHNS analyzer. The MALDI–TOF analysis was done on Voyager-De-STR MALDI–TOF (Applied Biosystems, Framingham, MA) equipped with 337-nm pulsed nitrogen laser used for desorption and ionization. A 1 μ M solution of the sample was premixed with DHB (2,5-dihydroxybenzoic acid) matrix in CHCl₃ and mixed well before spotting on 96-well stainless steel MALDI plate by dried droplet method for MALDI analysis. For small molecules SEC was performed using polystyrene standards for the calibration in CHCl₃ as eluent. The flow rate of CHCl₃ was maintained as 1 μ L/min throughout the experiments and the sample solutions at concentrations 3–4 mg/mL were filtered and injected for recording the chromatograms at 30 °C. The molecular weights of the polymers were determined by gel permeation chromatography (GPC), which was performed using a Viscotek VE 1122 pump, Viscotek VE 3580 RI detector, and Viscotek VE 3210 UV/vis detector in tetrahydrofuran (THF) using polystyrene as standards. UV–vis spectra were recorded using a Perkin-Elmer Lambda-35 UV–vis spectrometer. The thermal stability of all the model compounds and azo copolyesters were analyzed using a PerkinElmer:STA 6000 thermogravimetric analyzer (TGA) under nitrogen atmosphere from 40 to 900 °C at 50 °C/min. Differential scanning calorimetry (DSC) was performed using a TA Q10 model. 2–3 mg of the sample was taken in aluminum pan, sealed and scanned at 10 °C/min. The instrument was calibrated with indium standards before measurements. The phase behaviors of the molecules were analyzed using LIECA DM2500P polarized optical microscope equipped with Linkam TMS 94 heating and cooling stage connected to a Linkam TMS 600 temperature programmer. The transition from isotropic to liquid crystalline phase was monitored by the evolution of characteristic textures.

Photophysical Studies. Absorption spectra were recorded using Perkin-Elmer Lambda 35 UV-spectrophotometer. Steady-state fluorescence studies and time-resolved fluorescence lifetime measurements were performed using Horiba Jobin Yvon Fluorolog 3 spectrophotometer having a 450 W xenon lamp for steady-state fluorescence. Picosecond time-resolved-emission spectra (TRES) and fluorescence lifetime decays were collected by a time-correlated single photon counting (TCSPC) setup from IBH Horiba Jobin Yvon (U.S.) using a 375 nm diode laser (IBH, U.K., NanoLED-375 L, with a λ_{max} = 375 nm) having a fwhm of 89 ps as a sample excitation source. The

Scheme 1. Synthesis of Monomers and the Polymerization Scheme



emission and excitation slit width was maintained at 1 nm throughout the experiments, and the data was obtained in “S1c/R1” mode (to account for the variations in lamp intensity).

Transmission Electron Microscopy. For TEM measurements, the samples in THF were deposited directly on a carbon coated copper grid. No staining treatment was performed for the measurement. A JEOL JEM-3010 electron microscope operating at 300 kV ($C_s = 0.6$ mm, resolution 1.7 Å) was used for HR-TEM sample observation. A Gatan digital camera (model 794, Gatan 1024 × 1024 pixels, pixel size 24 × 24 μm) at 15 000–80 000× magnifications was used to record micrographs.

Atomic Force Microscopy. AFM images were taken by using a Multimode scanning probe microscope equipped with a Nanoscope IV controller from Veeco Instruments, Inc. in the tapping mode using a SiN probe, with a maximum scan size of 10 mm × 10 mm and with a vertical range of 2.5 mm. For the AFM studies, samples were prepared by drop-casting THF solution of the polymers onto the silicon wafer and allowed to dry at ambient temperature before being subjected to AFM analysis.

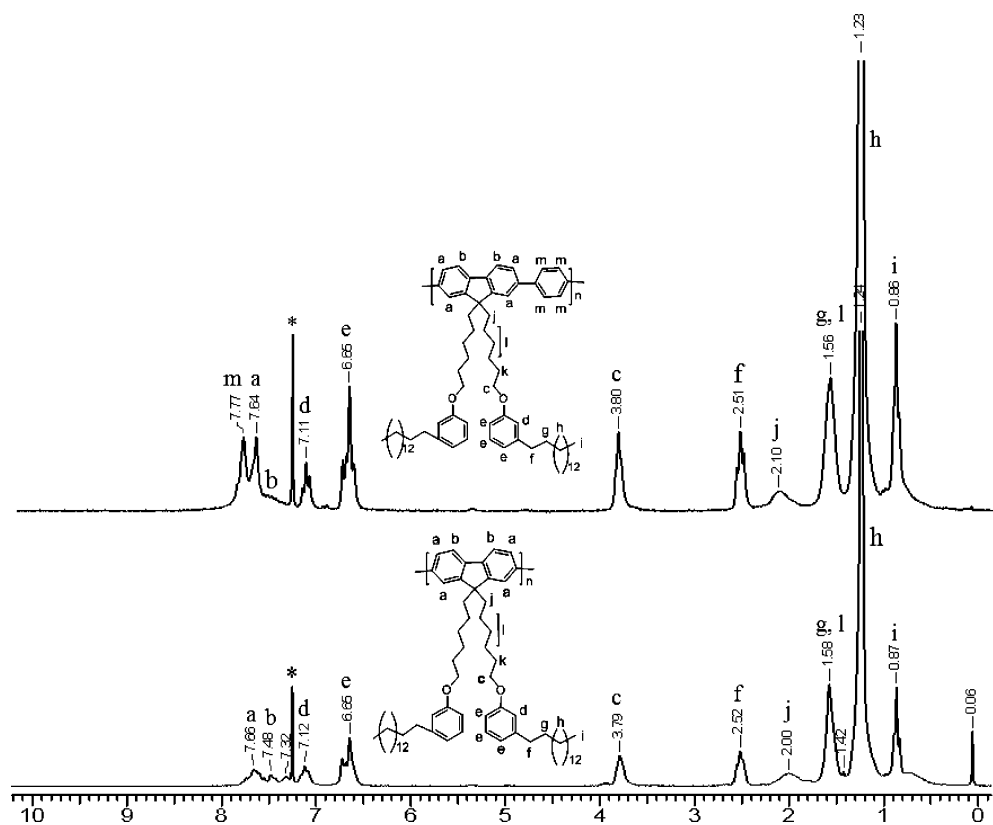
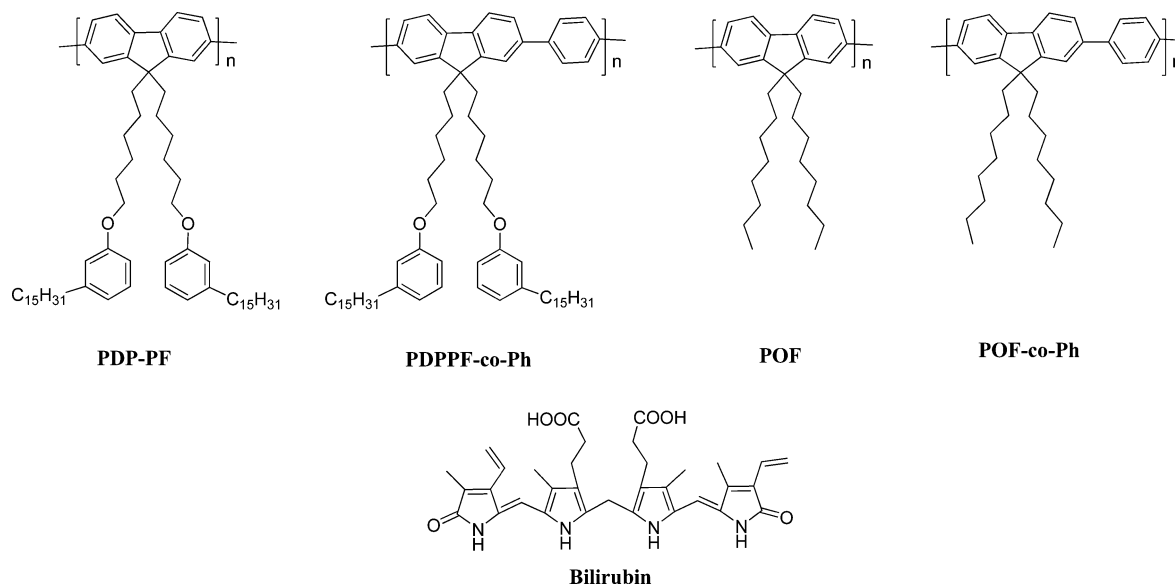
Dynamic and Static Light Scattering (DLS and SLS). DLS measurements were carried out on a Zetasizer ZS 90 apparatus, utilizing 633 nm red laser (at 90° angle) from Malvern Instruments. The reproducibility of the data was checked at least three times using independent polymer solutions.

The static light scattering experiment (SLS) was carried out using 3D-DLS spectrometer, from LS instruments, Switzerland. The instrument consists of a He Ne laser having wavelength of 632.8 nm attached to computer using the Lab view interface utilizing toluene as reference. The measurement was performed in autocorrelation mode from 20° to 134° by steps of 2°.

Synthesis of 1-(6-Bromohexyloxy)-3-pentadecylbenzene. 3-Pentadecylphenol (10 g, 3.29 mmol) and KOH (9.21 g, 16.4 mmol) were dissolved in ethanol (50 mL) and stirred for 30 min to obtain a reddish black precipitate. 1,6-Dibromohexane (25 mL, 16.4 mmol) in dry acetone (25 mL) was added very slowly to this reaction mixture and heated to reflux for 24 h. After cooling to room temperature, the solvent and excess 1,6-dibromohexane was distilled off and the product extracted with dichloromethane. The organic layer was washed with water, brine and dried with Na_2SO_4 . The solvent was removed under vacuum. The crude product was purified by silica gel column chromatography using pet ether/ethyl acetate (v/v, 97/3) as eluent to yield the product. Yield (18 g, 78%). $^1\text{H NMR}$ (CDCl_3 , 200 MHz): $\delta = 7.17$ (t, 1H), 6.72 (t, 3H), 3.94 (t, 2H), 3.42 (t, 2H), 2.56 (t, 2H), 1.9–1.7 (m, 4H), 1.50 (m, 6H), 1.35–1.15 (m, 24H), 0.87 (t, 3H).

Synthesis of 2,7-Dibromo-9,9-bis(6-(3-pentadecylphenoxy)hexyl)-9H-fluorene. (1). 2,7-dibromofluorene (3 g, 9.26 mmol) and NaH (2.22 g, 92.6 mmol) were taken in a two-necked round-bottom flask and purged with nitrogen. Dry THF (60 mL) was added to this to obtain a dark red precipitate. (6-Bromohexyloxy)-3-pentadecylbenzene (17.32 g, 37.04 mmol) was added very slowly to this reaction mixture and heated to reflux for 12 h. The reaction mixture was poured into water and the product was extracted with ethyl acetate. The organic layer was washed with water, brine, and dried over Na_2SO_4 . The solvent was removed under vacuum. The crude product was purified by silica gel column chromatography using pet ether/ethyl acetate (v/v, 95/5). Yield: 6.4 g (64%). $^1\text{H NMR}$ (CDCl_3 , 200 MHz): $\delta = 7.55$ –7.4 (m, 6H), 7.15 (t, 3H), 6.8–6.6 (m, 6H), 3.83 (t, 3H), 2.55 (t, 3H), 1.98–1.90 (m, 4H), 0.89 (t, 6H), 0.62 (m, 4H). MALDI (observed M^+ Na. 1119.67, calculated 1120.21.) Anal. Found: C, 59.53%; H, 7.31. Calcd: C, 59.71; H, 7.23.

Scheme 2. Structure of the Polyfluorenes and Bilirubin Used in the Study

Figure 1. ^1H NMR spectra of PDPPF-co-Ph and PDPF recorded in CDCl_3 .

Synthesis of 2,2'-(9,9-Bis(6-(3-pentadecylphenoxy)hexyl)-9H-fluorene-2,7-diyl)bis(4,4,5,5-tetramethyl-1,3,2-dioxaborolane) (2). 2,7-Dibromo-9,9-bis(6-(3-pentadecylphenoxy)hexyl)-9H-fluorene (1.35 g, 1.24 mmol) was dissolved in dry THF (20 mL) and cooled to -78°C . *n*-BuLi (1.5 mL, 2 M in hexane) was added dropwise over a period of 45 min to the above THF solution, and the reaction mixture was stirred for 1 h. At the same temperature, 2-isopropoxy-4,4,5,5-tetramethyl-1,3,2-dioxaborolane (0.7 mL, 4.93 mmol) was added over a period of 30 min and stirred for further 2 h. The reaction mixture was then slowly warmed to room temperature and stirred for 12 h. For work-up, the reaction was quenched with water (10 mL), and the reaction mixture was poured into water and

extracted with dichloromethane. The organic layer was washed with water and brine and dried over Na_2SO_4 . The solvent was removed under reduced pressure. The crude product was purified by silica gel column chromatography using pet ether/ethyl acetate (v/v, 90/10). Yield: 0.75 g (51%). ^1H NMR (CDCl_3 , 200 MHz): δ = 7.7–7.2 (m, 6H), 7.15 (t, 2H), 6.67 (m, 6H), 3.81 (t, 4H), 2.55 (t, 4H), 1.95 (m, 4H), 1.58 (m, 10H), 1.38 (s, 24H), 1.25 (m, 50H), 0.89 (t, 6H), 0.64 (m, 4H). MALDI: observed $M + \text{Na} = 1214.22$; calculated $M + \text{Na} = 1214.41$.

Polymerization. 2,7-Dibromo-9,9-bis(6-(3-pentadecylphenoxy)hexyl)-9H-fluorene (300 mg, 0.27 mmol), 2,2'-(9,9-bis(6-(3-

pentadecylphenoxy)hexyl)-9H-fluorene-2,7-diyl)bis(4,4,5,5-tetramethyl-1,3,2-dioxaborolane) (diboronic ester) (325 mg, 0.27 mmol) and tetrakis(triphenylphosphine) palladium (20 mg, 0.04 mmol) were taken into a two necked round-bottom flask under nitrogen atmosphere. Dry THF (8 mL) was added to the mixture. K_2CO_3 dissolved in water (2 mL) was added to the reaction medium. The reaction mixture was heated to reflux for 36 h under nitrogen atmosphere. The mixture was cooled down to room temperature and added dropwise into a stirred solution of methanol (100 mL) in an open vessel. The precipitate was isolated and dissolved in dichloromethane and filtered to remove the catalyst. The collected dichloromethane solution was concentrated under reduced pressure and purified by repeated precipitation from methanol (100 mL). The precipitate was filtered, washed with methanol (50 mL), and dried under high vacuum.

Poly[2,7-(9,9-bis(6-(3-pentadecylphenoxy)hexyl)-9H-fluorene)] (PDP–PF). 1H NMR ($CDCl_3$, 200 MHz): δ (ppm) 7.66 (4H, m), 7.48 (2H, m), 7.11 (2H, q), 6.65 (6H, m), 3.80 (4H, m), 2.51 (4H, m), 2.10 (4H, m), 1.58 (8H, m), 1.23 (60H, m), 0.87 (6H, m). Yield: 75%.

Poly[(1,4-phenylene)-2,7-(9,9-bis(6-(3-pentadecylphenoxy)hexyl)-9H-fluorene)] (PDPPF-co-Ph). The copolymer PDPPF-co-Ph was prepared by following the same procedure but using 1,4-benzene diboronic pinacolate ester as the comonomer. Yield: 78%. 1H NMR ($CDCl_3$, 200 MHz): δ (ppm) 7.77 (4H, m), 7.64 (4H, m), 7.48 (2H, m), 7.12 (2H, q), 6.65 (6H, m), 3.79 (4H, m), 2.52 (4H, m), 2.0 (4H, m), 1.58 (8H, m), 1.23 (60H, m), 0.87 (6H, m).

POF and POF–Ph were synthesized following literature procedures.²⁴

Poly[2,7-(9,9-dioctylfluorene)] (POF). 1H NMR ($CDCl_3$, 200 MHz): δ (ppm) 7.85 (2H, d), 7.68 (4H, m), 2.15 (4H, m), 1.2 (24H, m), 0.8 (6H, t). Yield: 80%.

Poly[(1,4-phenylene)-2,7-(9,9-dioctylfluorene)] (POF–Ph). 1H NMR ($CDCl_3$, 200 MHz): δ (ppm) 7.85 (4H, d), 7.65–7.5 (2H, m), 2.1 (4H, m), 1.15 (24H, m), 0.85 (6H, t). Yield: 75%.

RESULTS AND DISCUSSION

Synthesis and Characterization. The synthesis of PDP–PF and PDPPF-co-Ph are shown in Scheme 1. The dibromo monomer 2,7-dibromo-9,9-bis(6-(3-pentadecylphenoxy)hexyl)-9H-fluorene (**1**) and the dioxaborolane monomer, 2,2'-(9,9-bis(6-(3-pentadecylphenoxy)hexyl)-9H-fluorene-2,7-diyl)bis(4,4,5,5-tetramethyl-1,3,2-dioxaborolane) (**2**), were synthesized in 50–64% yield and the details of synthesis are given in the Experimental Section. The structure and purity of the monomers were confirmed by 1H NMR, MALDI, and elemental analysis (Supporting Information SI-1a–f). The 2,7-dibromo-9,9-dioctylfluorene and its boronic ester were synthesized following reported procedure.^{24,25} The Suzuki polymerization of the monomers **1** and **2** in the presence of $Pd(PPh_3)_4$ catalyst afforded poly(2,7-dimethyl-9,9-bis(6-(3-pentadecylphenoxy)hexyl)-9H-fluorene) (PDP–PF) in 75% yield. The monomer **1** was coupled with phenyl boronic ester to obtain the copolymer (PDPPF-co-Ph). Poly[2,7-diyl-(9,9-dioctylfluorene)] (POF) and its copolymer with a phenyl group, poly[(1,4-phenylene)-2,7-diyl-(9,9-dioctylfluorene)] (POF-co-Ph) were also synthesized as benchmark polymers to compare the photophysical and sensing properties. Scheme 2 shows the structure of all the polymers that were used in the present study along with the structure of bilirubin. Figure 1 compares the labeled proton NMR spectra of the PDP–PF and copolymer PDPPF-co-Ph. The broadening of the peaks in 1H NMR indicated reasonably high molecular weights. The number-average molecular weight (M_n) and polydispersity of the polymers were determined by gel permeation chromatography (GPC) using THF as solvent. The GPC chromatograms

of the polymers are given in Supporting Information, Figure SI-1e. The number and weight-average molecular weight (M_n , M_w), polydispersity index, yield and 10% weight loss temperature of the different polymers are given in Table 1. PDP–PF

Table 1. Sample Designation, Number and Weight Average Molar Mass, Polydispersity Indices, Yield and 10 Wt % Loss Temperature of the Polyfluorenes

polymer	number-average molecular weight (M_n) ^a	weight-average molecular weight (M_w) ^a	polydispersity index (D_M)	yield (%)	10% weight loss temperature (°C)
PDP–PF	19 600	53 000	3.5	75	370
PDPPF-co-Ph	18 600	46 000	2.4	78	408
POF	9000	22 000	2.4	80	420
POF-co-Ph	20 300	36 100	1.7	75	411

^aMeasured by size exclusion chromatography (SEC) in tetrahydrofuran (THF), calibrated with linear, narrow molecular weight distribution polystyrene standards.

had a M_w of 53,000 with a polydispersity index (D_M) of 3.5 and PDPPF-co-Ph had a M_w of 46,000 with a D_M of 2.4. The molecular weight and polydispersity values were comparable with the polyfluorenes reported in the literature.²⁵

Thermal Analysis and Liquid Crystallinity. The 10% weight loss temperature determined using TGA (plot given in Supporting Information, SI-1f) indicated that all polymers were thermally stable up to 350 °C. The family of dialkylpolyfluorenes is well-known for their ability to exhibit thermotropic nematic liquid crystalline phases.²⁶ The thermotropic liquid crystalline tendency of the PDP-based homo and copolymers PDP–PF and PDPPF-co-Ph were analyzed using both differential scanning calorimetry (DSC) and polarized light microscopy (PLM). Both polymers were sluggish to crystallize, therefore, they were subjected to rapid cooling from isotropic to -70 °C and then a heating and cooling cycle were recorded at a slow rate of 2 °C/min. The DSC thermograms and polarized optical microscopic images of PDP–PF and PDPPF-co-Ph in their second heating and cooling cycles respectively are given in Supporting Information (SI-2). PDP–PF showed a glass transition at -24 °C, followed by a sharp endothermic transition at -1.8 °C with an enthalpy of 9.3 J/g and a melting transition at 39 °C with an enthalpy of 0.95 J/g in the heating cycle. While cooling from the isotropic melt, a sharp crystallization was observed at -13 °C followed by a glass transition at -30 °C. PDPPF-co-Ph exhibited only one transition at -20 °C both in the heating and cooling cycle as seen in the DSC thermogram. Clear nematic thread-like patterns of PDP–PF and PDPPF-co-Ph polymers could be observed under the PLM after rapid quenching of the isotropic sample using liquid nitrogen. Observation under the PLM indicated that PDP–PF melted at around 40 °C whereas PDPPF-co-Ph melted at a higher temperature of 116 °C. Sluggishness of the polymers PDP–PF and PDPPF-co-Ph to crystallize is ascribed to the increasing flexibility imparted by the pentadecyl units.²⁷

Self-Assembly. The PDP-substituted polyfluorene has a rod-coil structure with the rigid polyfluorene backbone forming the rod segment and the hexyloxy appended PDP unit forming the coil segment. In general, rod-coil structures modified with hydrophilic and hydrophobic groups have been

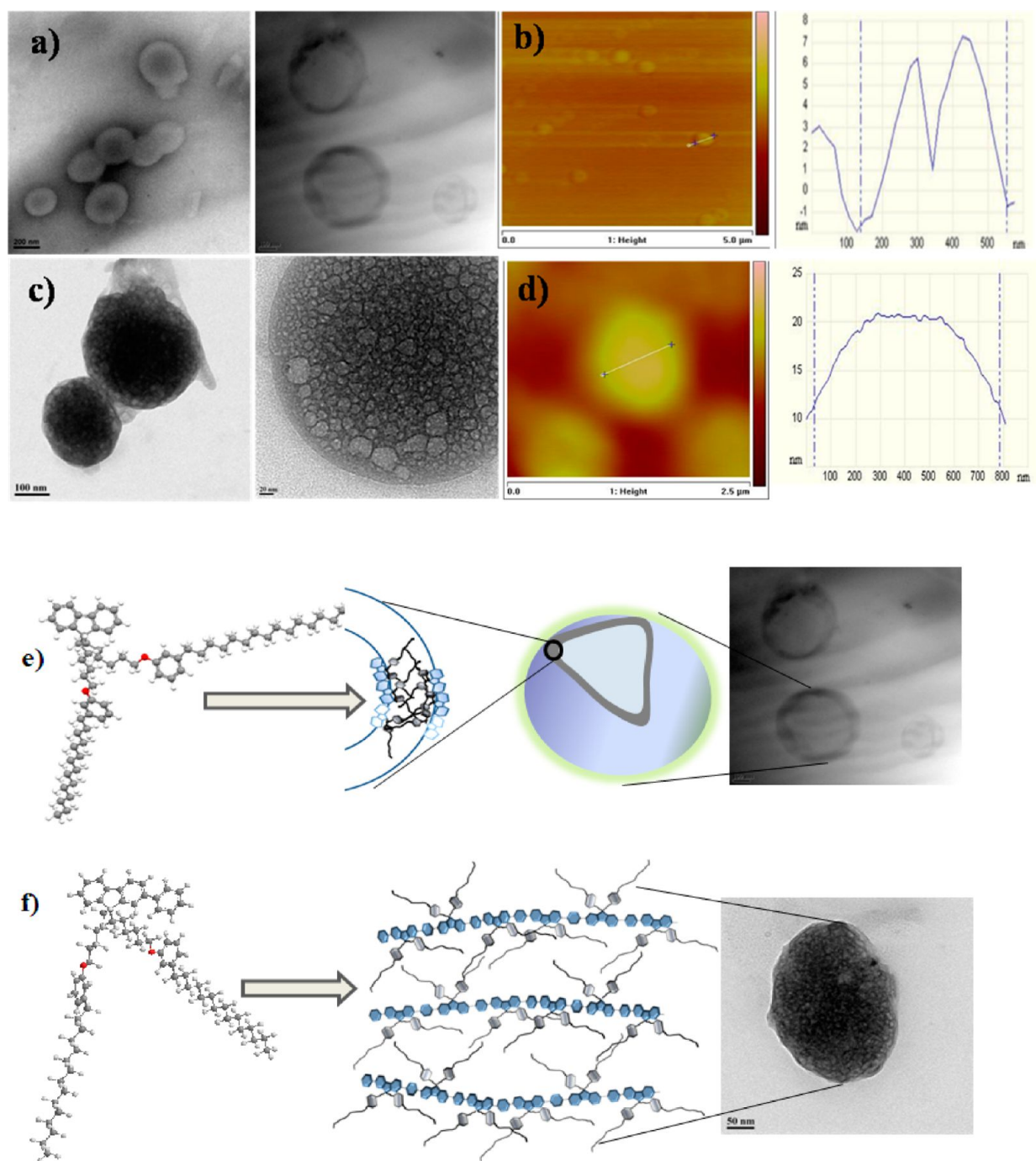


Figure 2. (a, c) TEM images of **PDP-PF** (top) and **PDPPF-co-Ph** (bottom) at 1×10^{-5} M concentration drop cast on carbon coated copper grids. (b, d) Tapping mode AFM images of **PDP-PF** (top) and **PDPPF-co-Ph** (bottom) at 1×10^{-5} M concentration coated on silicon wafers. The corresponding height section analysis are also shown. (e, f) Schematic diagram showing the self-assembly of **PDP-PF** and **PDPPF-co-Ph** into vesicles and porous spherical aggregates.

shown to exhibit nanophase separation into various morphologies. Dialkyl-substituted polyfluorenes, in particular 9,9-dioctylfluorene, have been shown to self-assemble into hairy rod structures,²⁸ whereas polyfluorenes with poly(ethylene oxide) side chains have been shown to form fluorescent micellar structures in aqueous solution.²⁹ The self-assembly behavior of the two polymers **PDP-PF** and **PDPPF-co-Ph** in tetrahydrofuran (THF) as solvent was studied. Both polymers had good solubility in THF and a 1×10^{-5} M solution in THF was drop cast onto TEM grids and the solvent was allowed to

evaporate at room temperature. **PDP-PF** formed vesicles with an average diameter of 300–500 nm as shown in Figure 2a top where a thin wall could be clearly differentiated by the dark contrast. AFM was also recorded by casting the sample in THF onto silicon wafers. Figure 2b shows the tapping-mode AFM height profile clearly showing spheres with a small crater-like depression characteristic of vesicles. The average diameter observed from AFM was around 400 nm. In sharp contrast, the **PDPPF-co-Ph** formed soap bubble-like porous spherical structures with average diameter of 300–700 nm (Figure 2c).

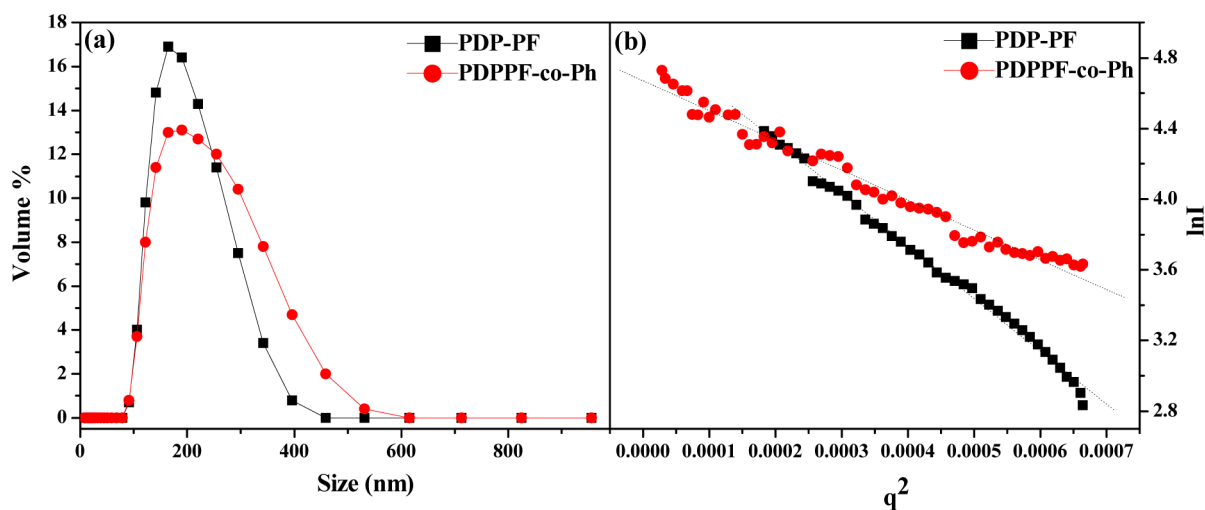


Figure 3. (a) Volume-average size distribution of the two polymers **PDP-PF** and **PDPPF-co-Ph** in THF (5×10^{-6} M) obtained by dynamic light scattering (DLS) analysis. (b) Static light scattering (Guinier plot) for **PDP-PF** and **PDPPF-co-Ph** (5×10^{-6} M) in THF.

More TEM images of the porous structures of **PDPPF-co-Ph** and vesicles of **PDP-PF** are given in Supporting Information (SI-3). The AFM height profile (Figure 2d) also clearly distinguished them as spheres and not vesicles.

Energy minimization was carried out for one repeat unit of **PDP-PF** and **PDPPF-co-Ph** using DFT,^{30,31} which showed that the PDP unit in **PDP-PF** with the C15 alkyl chain was extended outward resulting in a torsion angle of $\sim 62^\circ$ with the plane of the fluorene ring. The presence of two hexyloxy pentadecyl phenyl units on each repeating unit could be expected to put a strain on the polyfluorene backbone resulting in reduced conjugation of the backbone. This was proved by the blue shift in the absorption spectra of **PDP-PF** compared to **POF**, as discussed later on. Figure 2e shows a schematic diagram representing the self-assembly of **PDP-PF** into vesicles. Bilayer structures are formed by the interdigitation of the C15 alkyl chains of the PDP units, which would further transform into vesicles due to the curvature formed by twisting of the strained polyfluorene backbone. The extra phenyl ring on each repeating unit of the polyfluorene backbone in the case of **PDPPF-co-Ph** could be expected to lessen the strain felt by the backbone leading to a more open porous structure with accessible interior volumes. Figure 2f shows the schematic representation of self-assembly in **PDPPF-co-Ph** resulting in formation of open and interconnected porous spheres. Small structural changes in fluorene oligomers have been shown to result in differences in torsion angles between neighboring units and different molecular shapes eventually resulting in strong differences in aggregation behavior.^{32,33} The differences in the extent of twisting/torsion angle of the polyfluorene backbone is expected to be the driving force causing strong differences in the mode of self-assembly in the two polymers **PDP-PF** and **PDPPF-co-Ph**.

Rod-coil polymers are known to exist in self-assembled vesicles and micelles in solution and to retain these structures in film form upon evaporation of solvent.³⁴ Information regarding the size and morphology of the particles in solution can be obtained from dynamic and static light scattering experiments (DLS and SLS).³⁵ Dynamic light scattering (DLS) analysis in THF showed a good autocorrelation and indicated presence of particles with average diameter ~ 200 and 260 nm for **PDP-PF** and **PDPPF-co-Ph** polymers as shown in Figure

3a. This was in good correlation with the size obtained from TEM and AFM measurements. The slight increase in size of the self-assembled structures in film is probably due to aggregation upon solvent evaporation. The hydrodynamic radius (R_H) of 96 and 99 nm was extracted from the dynamic light scattering experiments for **PDPPF-co-Ph** and **PDP-PF** respectively. In the static light scattering experiment, the intensity of the scattered light measured at different angles is plotted against q^2 , where q is the magnitude of the scattering vector. This plot known as the Guinier plot is shown in Figure 3b for **PDPPF-co-Ph** and **PDP-PF**. R_g values of 73 and 95 nm were obtained for **PDPPF-co-Ph** and **PDP-PF** respectively. The ratio between R_g/R_H obtained from the static and dynamic light scattering experiments respectively, called shape factor (ρ) is a well-known indicator for the morphology of the assemblies in solution ($\rho \sim 0.77$ for hard sphere, $\rho \sim 1$ for vesicles, and $\rho \sim 1.7$ for the coil conformation).³⁶ The ratio R_g/R_H was obtained as 0.76 for **PDPPF-co-Ph** and 0.96 for **PDP-PF** confirming the existence of spherical particles for the former and vesicles for the latter in solution. Thus, the observations from the light scattering experiments strongly supported the morphology observed using the various microscopic techniques.

Photophysical Properties. Figure 4 depicts the absorption and emission characteristics of all the polymers used in the present study in THF solvent along with that of the absorption spectrum of bilirubin. The characteristic broad featureless absorption of the polymers with absorption maxima at 350 and 366 nm for **PDP-PF** and **PDPPF-co-Ph** respectively is assigned to the $\pi-\pi^*$ transition of the polyfluorene backbone. Compared to the absorption of dialkyl-substituted polyfluorenes like 9,9'-dioctylpolyfluorene which has absorption wavelength maxima at 383 nm, the absorption maximum of **PDP-PF** was blue-shifted by 33 nm. The introduction of bulky hexyloxy pentadecyl phenol unit twisted the polyfluorene backbone resulting in reduced conjugation length as indicated by the DFT energy minimized structure discussed earlier. The degree of backbone twisting was lessened in the case of copolymer **PDPPF-co-Ph** because of the presence of the rigid phenyl unit. Figure 4 also compares the normalized emission spectra (dotted lines) of the polymers in THF upon excitation at their absorption wavelength maxima. The polymers exhibited emission spectra with clear vibronic transitions at 409, 432, and

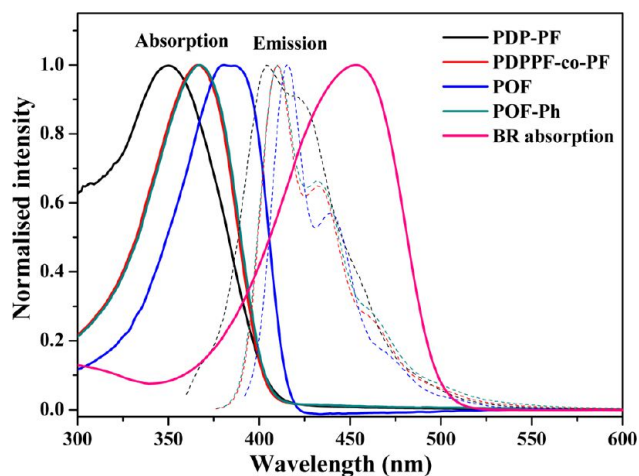


Figure 4. Stack plot of normalized absorption and emission spectra of all polymers along with the absorption spectrum of bilirubin in THF. Polymers were excited at the respective absorption wavelength maxima.

462 nm for PDPPF-*co*-Ph and at 404, 422, and 456 nm for PDP-PF corresponding to 0–0, 0–1, and 0–2 transitions respectively from the lowest singlet excited state. The fluorescence quantum yield of the two polymers PDP-Ph and PDPPF-*co*-Ph along with that of POF and POF-*co*-Ph polymers were determined using 0.1 OD solutions in THF relative to quinine sulfate ($\Phi_{\text{fl}} = 0.546$) as the reference and the data is given in Table 2. The PDPPF-*co*-Ph exhibited the

Table 2. Fluorescence Quantum Yields Φ_{PF} , Spectral Overlap Integral $J(\lambda)$, Förster Radii R_0 , and Energy Transfer Efficiency of the Donor Polyfluorenes with Bilirubin as Acceptor together with the Calculated Donor–Acceptor Distance (r)

donor polymer	Φ_{PF}^a	$J(\lambda) 10^{15}$ ($\text{M}^{-1} \text{cm}^{-1}$ (nm^4))	Förster distance R_0 (Å)	energy transfer efficiency (%)	donor–acceptor distance r (Å)
PDP-PF	0.61	1.04	46.16	52	45.55
PDPPF- <i>co</i> -PF	0.78	1.40	48.99	86	36.2
POF	0.72	1.50	50.42	33	56.7
POF- <i>co</i> -Ph	0.66	1.38	50.50	43	51.39

^aThe fluorescence quantum yields were obtained using 0.1 OD quinine sulfate ($\Phi = 0.546$) solution at 360 nm in 0.1 M H_2SO_4 solution as a standard.

highest quantum yield of 78%, whereas PDP-PF had a quantum yield of $\sim 61\%$ only. Although bulky groups are known to enhance the quantum yield significantly by retarding detrimental polymeric aggregation,³⁷ if the bulky groups result in considerable twisting of the conjugated polymer backbone the result would be a reduction in emission efficiency and quantum yield.³⁸

Fluorescence Sensing of Bilirubin. The targeted analyte molecule bilirubin (structure shown in Scheme 2) undergoes structural isomerization into another isomer (lumirubin) upon prolonged exposure to light.³⁹ Hence all our photophysical studies with bilirubin in THF were carried out in dim light and bilirubin stock solutions were kept away from light and stored below room temperature ($\sim 10^\circ\text{C}$). The emission spectra of

PDP-PF and PDPPF-*co*-Ph showed good overlap with the absorption spectra of bilirubin (shown in Figure 4) indicating the possibility of fluorescence resonance energy transfer (FRET) from polymer to bilirubin. Figure 5a shows the effect of addition of varying concentrations of bilirubin (0.1×10^{-6} to 10×10^{-6} M) on the absorption spectra of PDPPF-*co*-Ph (5×10^{-6} M). No change was observed in the absorption spectra of polyfluorene upon addition of bilirubin, but a new peak at 453 nm corresponding to bilirubin absorption became more prominent at higher concentrations of bilirubin. Figure 5b shows the corresponding emission spectra, upon excitation at 367 nm. On addition of bilirubin, there was a drastic reduction in the characteristic emission of polymer at 410 nm. The inset in Figure 5b shows the same figure with the unquenched emission of PDPPF-*co*-Ph removed for better clarity. Figure 5c shows the same spectra after normalizing at polyfluorene emission maxima highlighting the FRET-induced bilirubin emission at 502 nm. Bilirubin is known to emit at 502 nm with low quantum efficiency (<0.00002 at 25°C in (CHCl_3)).⁴⁰ The bilirubin emission at 502 nm increased in the intensity with obvious color change in solution from blue to green. The inset in Figure 5c shows photographs taken under a hand-held UV lamp highlighting the visual color change at various intervals of addition of bilirubin. The gradual evolution of color change upon addition of bilirubin to PDPPF-*co*-Ph is also explained using the CIE diagram where the emission at various concentrations was plotted in the CIE graphical representation in Supporting Information (SI-4). This visual color change makes quick and easy monitoring of bilirubin levels a reality. The gradual color change with varying concentration of bilirubin signals the corresponding change from normal to abnormal levels of bilirubin.

Similar fluorescence quenching experiments were conducted for PDP-PF and also for the dioctyl substituted benchmark polymers POF and POF-*co*-PH and are given in the Supporting Information, SI-5. Figure 5d compares the change in fluorescence intensity for the four polymers as a function of varying bilirubin to polymer concentration. There was a 10-fold reduction in the emission of PDPPF-*co*-Ph for 0.1 mol % addition of bilirubin. The homopolymer PDP-PF also showed a reduction in emission intensity upon addition of bilirubin although the reduction was gradual and not drastic as in the case of the phenyl copolymer PDPPF-*co*-Ph. Compared to the PDP substituted polyfluorenes, the performance of the poly 9, 9-dioctylfluorene homopolymer (POF) and copolymer (POF-*co*-Ph) were very poor with marginal decrease in emission intensity. The quenching of polymer fluorescence upon addition of bilirubin was not accompanied by changes in the polymer absorption spectra (or excitation spectra; see Supporting Information, SI-6) which ruled out charge transfer between polymer and bilirubin. The good overlap in the emission spectra of polymer and absorption spectra of bilirubin suggested energy transfer as the most plausible reason for the quenching of polymer fluorescence. The FRET ratio calculated as the ratio of integrated area of bilirubin emission from 482 to 700 nm to that of polyfluorene emission in the range 360 to 482 nm for the four polymers as a function of increasing bilirubin concentration was compared in Figure 5e. At all bilirubin concentrations, PDPPF-*co*-Ph exhibited the highest FRET efficiency compared to the other polymers. The FRET efficiency at higher bilirubin concentrations was ~ 7 times higher for PDPPF-*co*-Ph compared to the PDP-PF.

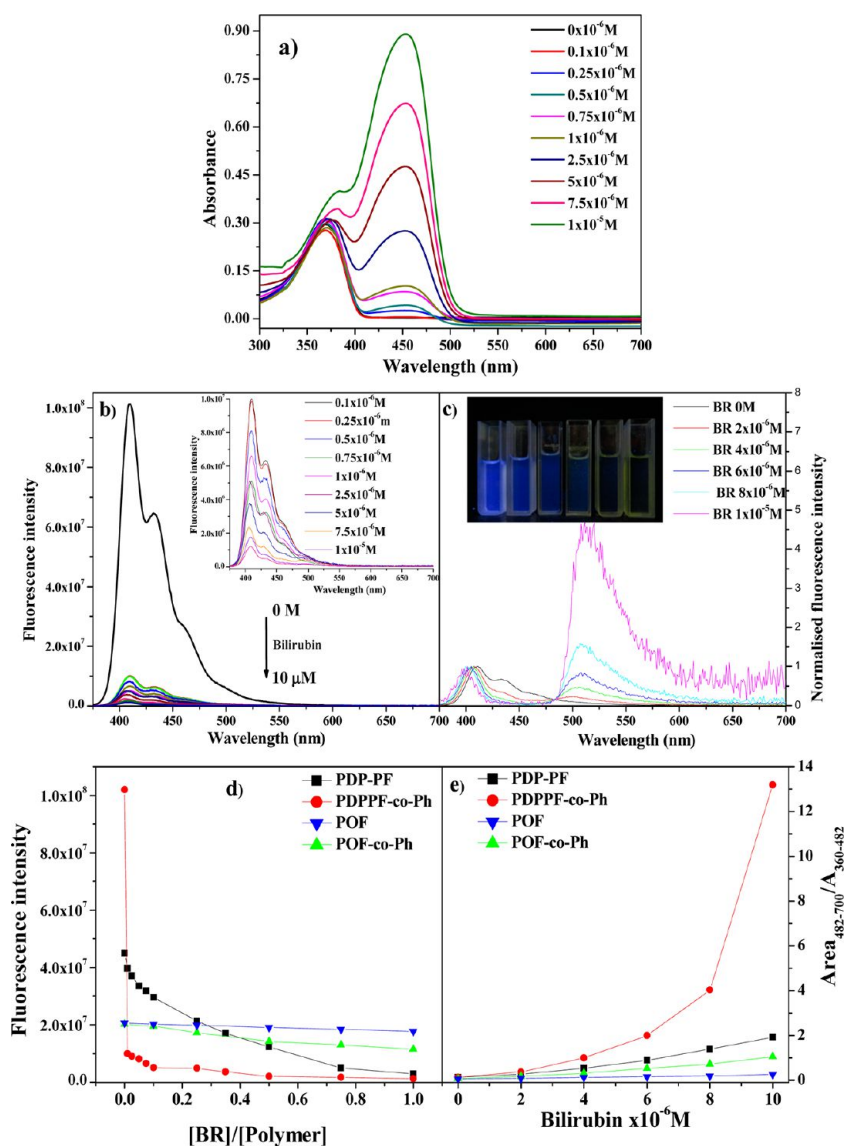


Figure 5. (a) Absorption spectra of PDPFF-*co*-Ph (5×10^{-6} M) upon addition of various concentrations of bilirubin (0.1×10^{-6} M to 1×10^{-5} M) in THF. (b) Fluorescence spectra of PDPFF-*co*-Ph (5×10^{-6} M) upon addition of various concentrations of bilirubin (0.1×10^{-6} to 1×10^{-5} M) in THF. Inset shows the same figure without the initial unquenched emission of PDPFF-*co*-Ph. Excitation wavelength was 367 nm. (c) Normalized (~ 410 nm) emission spectra highlighting the FRET-induced bilirubin emission at 502 nm. Inset shows the photograph of the emission observed under a hand-held UV lamp. (d) Fluorescence intensity of polymers at 410 nm as a function of [bilirubin]/[polymer] ratio. (e) FRET ratio (integrated area of bilirubin emission to that of polyfluorene emission; $A_{BR(482-700)}/A_{PF(360-482)}$) of the polymers at various concentration of bilirubin.

Since FRET is a distance-dependent radiationless transfer of energy from a donor to acceptor molecule it can be used to investigate molecular interactions between the donor and acceptor. The FRET efficiency is good for donor–acceptor distances in the range of ~ 10 – 100 Å and it depends on the spectral overlap of the donor emission and the acceptor absorption (spectral overlap integral “ J ”) and the relative orientation of the donor and acceptor transition dipole moments (orientation factor “ k ”) must be approximately parallel. The various parameters for calculating donor–acceptor distance (r) like the spectral overlap integral $J(\lambda)$, Förster distance (R_0), and energy transfer efficiency (E) were calculated for 0.1 OD solutions of the polyfluorenes in the absence and presence of bilirubin (1×10^{-5} M) in THF (Supporting Information, SI-7) and the calculated values are given in Table 2. Details of the calculations and the equations used are given in the Supporting Information. The energy transfer was highest

for the PDP-*co*-Ph polymer with a maximum value of 86% followed by the PDP–PF homo polymer (52%). POF and POF-*co*-Ph gave efficiency values of 43% and 33%, respectively. The energy transfer efficiency is related to the Förster distance by eq 2 in the Supporting Information. The Förster distances for the four polymers were similar and in the range of 46–50 Å, which was within the maximum separation distance (20–60 Å) between donor and acceptor over which resonance energy transfer can occur.⁴¹ From the known values of E and R_0 , the actual distance between the donor and acceptor—“ r ” was determined using eq 1 in the Supporting Information and is shown in Table 2. Comparing the values of the donor–acceptor distances of the four polymers it can be seen that PDPFF-*co*-Ph had the shortest distance of ~ 36 Å, whereas the other polymers had larger D–A distances (>45 Å).

On the basis of these observations a plausible mechanism of sensing is depicted schematically in Figure 6. The spectral

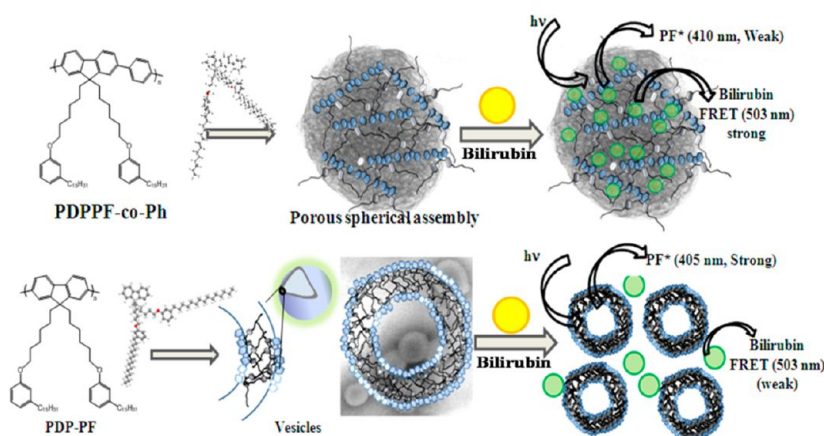


Figure 6. Schematic representation of the mechanism of FRET-induced bilirubin sensing in PDPPF-co-Ph and PDP-PF.

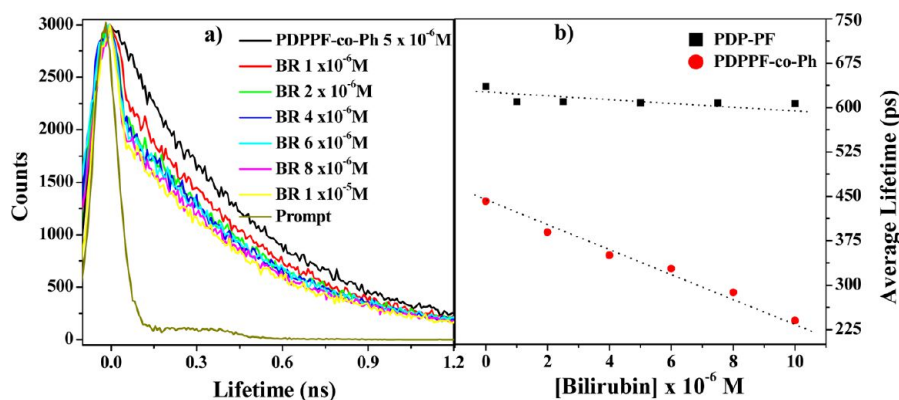


Figure 7. (a) Fluorescence lifetime measurement for the polymer [PDPPF-co-Ph] = 5×10^{-6} M at various Bilirubin concentration (1×10^{-6} M to 1×10^{-5} M) collected at 410 nm by using nanoLED of 375 nm. (b) Plot of the average lifetime of PDP-PF and PDPPF-co-Ph as a function of bilirubin concentration.

overlap of the polyfluorene emission with bilirubin absorption was in the similar range for all the polymers used in the present study. The physical proximity of the analyte to the polymer is a major deciding factor in these energy transfer processes. Figure 6 depicts the open porous spherical self-assembled aggregates of PDPPD-co-Ph which allows easy access to the bilirubin molecules whose diameter ranges <5 nm,⁴² into the interior of the spherical assembly ($r_{PF-BR} \sim 36$ Å). This results in a more efficient transfer of energy from PF to BR upon excitation of PF. On the other hand, the closed vesicular assembly of PDP-PF allows interaction of BR only on the periphery. BR cannot penetrate the clear demarcating walls of the polymer vesicles limiting their proximity to $r_{PF-BR} > 45$ Å. The synergistic effect of morphology and efficient energy transfer thus acts in favor of PDPPD-co-Ph enabling naked eye detection of bilirubin using hand-held UV lamp.

Fluorescence Lifetime Studies. Fluorescence lifetime of the polyfluorenes was obtained by picosecond time-correlated single photon counting (TCSPC) technique. Time resolved fluorescence decays were collected at 410 nm (polyfluorene emission) with excitation at 375 nm in THF as solvent at 25 °C. The lifetime decay analysis of bilirubin could not be carried out due to the very weak nature of its fluorescence. Polyfluorenes are known to exhibit complex fluorescence decay behavior in solution which is both solvent and temperature dependent.⁴³ The fluorescence decay of PDPPF-co-Ph could be fitted to a biexponential fit with lifetimes of 211

ps (0.35%) and 495 ps (0.65%) ($\chi^2 = 1.005$). The lifetime reduced sharply with increasing bilirubin concentration reaching biexponential fit values of 38 ps (0.30%) and 253 ps (0.70%) ($\chi^2 = 1.06$) for the highest bilirubin content of 1×10^{-5} M. Figure 7a shows the time-resolved fluorescence decay of PDPPF-co-Ph upon addition of varying concentrations of bilirubin. The decay of the polymer alone in the absence of bilirubin is also given for comparison. A sharp change in the decay pattern identifiable as two distinct regions – one where the slope was similar to that of the polymer alone (>0.2 ps) and the other where the slope changed with the different bilirubin concentration (<0.2 ps) was clearly discernible in the PDPPF-co-Ph bilirubin system. Similar time-resolved fluorescence decay was collected for the all other polymers also upon addition of varying amounts of bilirubin (given in Supporting Information, Table S1). The average lifetime ($\langle \tau \rangle$) calculated as $\langle \tau \rangle = \sum a_i \tau_i^2 / \sum a_i \tau_i$ ⁴⁴ (where “a” is the amplitude (normalized contribution)), was plotted as a function of bilirubin concentration for the two PDP substituted polyfluorenes and given in Figure 7b. It clearly showed that the average fluorescence lifetime of the homopolymer PDP-PF did not decrease much upon bilirubin addition; in fact, after the first addition of bilirubin the lifetime remained constant indicating very low energy transfer. On the other hand, the drastic reduction in the average fluorescence lifetime in the case of PDPPF-co-Ph upon addition of bilirubin clearly gave evidence

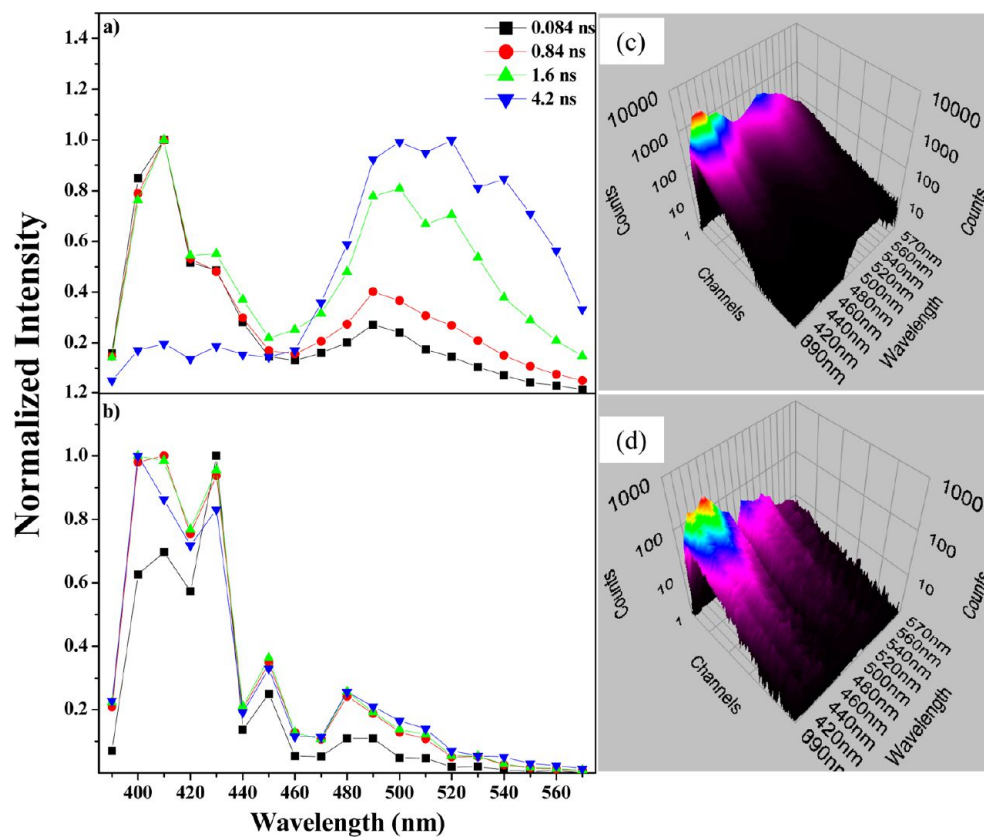


Figure 8. The normalized (at the wavelength of maximum fluorescence intensity) TRES with a gated time from 0.084 to 4.2 ns: (a) PDPPF-*co*-Ph and (b) PDP-PF. (c, d) Contour plots representing the three-dimensional time–intensity–wavelength data collected in the wavelength range 390 to 570 nm using nano LED of 375 nm.

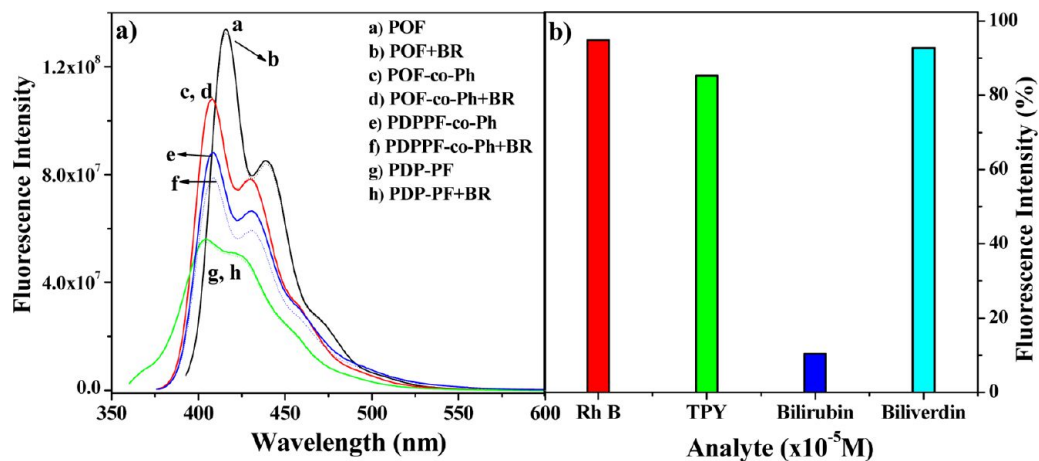


Figure 9. (a) Nanomolar sensing of all polymers. [polymer] = 1×10^{-5} M and [bilirubin] = 1×10^{-9} M. (b) Bar graph denoting fluorescence emission response profiles of PDPPF-*co*-Ph on addition of various analytes. [PDPPF-*co*-Ph] = 0.1 OD M, [analyte] = 1×10^{-5} M.

for efficient fluorescence energy transfer from polymer to bilirubin.

Additional insight into the different energy transfer efficiency of the two polymers PDP-*co*-Ph and PDP-PF toward bilirubin was obtained using time-resolved emission spectra (TRES) based experiments. In the picosecond TRES experiment the time-resolved decays at a number of wavelength (390–570 nm) across the emission spectrum were collected after the addition of 1×10^{-6} M bilirubin to a 5×10^{-6} M solution of the polymer in THF. A two-dimensional fluorescence emission spectra was constructed from the intensities sampled at discrete

times (0.084 to 4.2 ns) during the fluorescence decay. Figure 8 a, b compares the reconstructed normalized (at the wavelength of maximum emission) TRES for PDP-*co*-Ph and PDP-PF respectively during the time 0.084 to 4.2 ns, which was very similar to the normalized emission spectra in presence of bilirubin. The steady increase in the evolution of the bilirubin emission beyond 500 nm as a function of time could be clearly observed. Beyond 4.0 ns the polymer fluorescence was almost completely quenched and the bilirubin emission had increased 4-fold in the case of PDPPF-*co*-Ph. In sharp contrast, the same time gated spectra for PDP-PF showed that the polymer

emission was quite high compared to bilirubin emission, which clearly demonstrated the poor energy transfer efficiency of **PDP-PF** toward bilirubin compared to the copolymer **PDPPF-co-Ph**. Parts c and d of Figure 8 also show the contour plots representing the three-dimensional time-intensity-wavelength data showing the evolution of the FRET-induced bilirubin emission.

Sensitivity and Selectivity. The sensitivity of the bilirubin sensing was determined by adding nanomolar (1×10^{-9} M) solution of bilirubin to the polymers **PDP-PF**, **PDPPF-co-Ph**, **POF**, and **POF-co-Ph** (concentration of the polymers: 1×10^{-5} M), followed by excitation at the respective absorption wavelength maximum. Figure 9a compares the fluorescence spectra of the four polymers before and after addition of nanomolar concentration of bilirubin. Among all the polymers **PDPPF-co-Ph** showed the highest fluorescence quenching of 11% for nanomolar concentrations of bilirubin (1×10^{-9} M) where as no fluorescence quenching was observed at this low level of bilirubin in the case of the other polymers.

The selectivity of **PDPPF-co-Ph** toward bilirubin was investigated by analyzing sensing activity with structural analogues of bilirubin like biliverdin and dyes like 5,10,15,20-tetrapyrrolyl-23(*H*),25(*H*)-porphine (TPY) and rhodamine-B (Supporting Information, SI-8). Biliverdin, which is another heme residue co exists with bilirubin in plasma and bile and is the structural analogue of bilirubin with a double bond at the C10 position.⁴⁵ The electronic absorption spectrum of biliverdin has two peak maxima at 376 and 666 nm and it is a nonfluorescent molecule. The spectral overlap for the polyfluorene emission and the biliverdin absorption is almost negligible. 5,10,15,20-tetra(4-pyridyl)-23*H*-25*H*-porphine (TPY) is another structurally similar molecule, which can be considered as the closed ring analogue of bilirubin. Their absorption spectrum matches with the emission of the **PDPPF-co-Ph** given in Supporting Information. Figure 9b compares the percentage reduction of polymer (0.1 OD) fluorescence upon addition of 1×10^{-5} M of various analytes such as bilirubin, biliverdin, TPY and rhodamine B dye. Pronounced selectivity was observed only for bilirubin as analyte compared to the other structural analogues. This confirmed that the polymer **PDPPF-co-Ph** had pronounced selectivity for bilirubin. Biliverdin, the important structural analogue of bilirubin was unable to quench the polymer fluorescence even at higher concentrations.

Sensing in Water Medium. Under normal physiological conditions bilirubin is present in the conjugated form as di- and monoglucuronides (water-soluble) along with small amounts of unconjugated bilirubin (water insoluble).³⁹ The ability to sense the unconjugated or free fraction of bilirubin in presence of the water-soluble conjugated bilirubin, is a more challenging task. The unconjugated bilirubin is insoluble in water because of its ridge tile conformation.¹⁷ Literature reports the preparation of Bilirubin stock solution in water by dissolving known amount of bilirubin in presence of 10 mmol of NaOH.²³ An experiment was designed to simulate the bilirubin equilibrium in its water-soluble conjugated form and water insoluble unconjugated form by carrying out the sensing experiments in THF/water (containing NaOH) media. Varying amounts (1×10^{-6} M to 1×10^{-5} M) of sodium salt of bilirubin were prepared in water. The polyfluorene probe **PDPPF-co-Ph** being insoluble in water was taken in THF (8×10^{-6} M). Separate experiments were carried out where the polymer concentration was kept fixed and the water solution of bilirubin (of different concentrations) was

added to it. Care was taken to see that the polymer aggregation did not occur under the studied experimental conditions. For instance, it was observed that the photophysical properties of the polymer did not vary until a THF/water ratio of 6:4. Beyond this volume ratio, polymer aggregate emission at 550 nm appeared which would be detrimental in sensing experiments. Therefore, the THF/water ratio was fixed at (7.5: 2.5) to be on the safe side to avoid polymer aggregation. The sodium salt of the bilirubin in water was added in increasing amounts (1×10^{-6} M to 1×10^{-5} M) to the polymer solution in THF. Quenching of polymer fluorescence was observed (Supporting Information, SI-9) upon addition of bilirubin, which was due to the partitioning of bilirubin between water and THF. It was obvious that the probe was sensitive only to the free bilirubin present in the organic medium due to the polymers insolubility in the aqueous medium. Although, this partitioning of bilirubin between organic and aqueous medium was not a true reflection of the actual concentrations present in body fluids, the experiment was conducted to demonstrate the probable ability of the polymer to sense free bilirubin in the presence of conjugated form of bilirubin also. Further experiments are ongoing to develop a fully water-soluble polyfluorene probe which could be used for sensing albumin conjugated bilirubin.

CONCLUSIONS

In summary, pentadecylphenol-appended polyfluorene homopolymer (**PDP-PF**) and phenyl copolymer (**PDPPD-co-Ph**) were synthesized and characterized. The sensing efficiency of both polymers toward the biologically important analyte bilirubin was demonstrated by the quenching of polymer fluorescence and FRET-based bilirubin emission. Although, both polymers showed good overlap of their respective emission spectra with the absorption spectra of bilirubin, higher extent of quenching of polyfluorene emission at 410 nm (86%) together with increased bilirubin emission at 502 nm (5 times) was observed only in the case of **PDPPD-co-Ph**. The change in emission color from blue to green upon addition of bilirubin could be easily detected using a hand-held UV lamp. The differential self-assembling tendency of the polymers—open porous interconnected spherical assembly of **PDPPD-co-Ph** versus vesicles for **PDP-PF**—proved to play a crucial role in their energy transfer efficiencies. A short donor (polyfluorene) to acceptor (bilirubin) distance of 36 \AA was obtained for **PDPPD-co-Ph** in contrast to 46 \AA for **PDP-PF** using steady state fluorescence-based calculations. Fluorescence lifetime decay measurements also showed a significant reduction in the average lifetimes of **PDPPD-co-Ph** upon addition of bilirubin. The sensitivity of bilirubin detection by **PDPPD-co-Ph** polymer was tested using nanomolar concentrations of bilirubin. **PDPPD-co-Ph** exhibited a 11% quenching of its fluorescence upon addition of a 1×10^{-9} M solution of bilirubin, whereas **PDP-PF** and dioctyl substituted bench mark polyfluorene polymers did not exhibit any sensitivity to the presence of bilirubin at such low concentrations. The selectivity of detection was also investigated using structural analogues of bilirubin like biliverdin and dyes like 5,10,15,20-tetrapyrrolyl-23(*H*),25(*H*)-porphine (TPY) and rhodamine-B. Pronounced selectivity was observed only for bilirubin as analyte compared to the other structural analogues. We have thus highlighted the successful application of tailor-made highly fluorescent conjugated polymer based on polyfluorene for the sensitive

and selective sensing of bilirubin using hand-held UV lamp or a laboratory fluorimeter.

■ ASSOCIATED CONTENT

● Supporting Information

Details of structural characterization of the monomers and polymers and FRET-based calculations. This material is available free of charge via the Internet at <http://pubs.acs.org/>.

■ AUTHOR INFORMATION

Corresponding Author

*E-mail: sk.asha@ncl.res.in. Fax: 0091-20-25902615.

Notes

The authors declare no competing financial interest.

■ ACKNOWLEDGMENTS

This work has been financially supported by the network project NWP0054. The authors would like to thank Dr. Partha Hazra, IISER-Pune for TRES and Fluorescence Lifetime facility and Dr. Suresh Bhat, NCL-Pune for the Static light scattering measurements. The authors also thank Mr. Anuj, Mrs. Pooja, and Mr. Pankaj at NCL-Pune for the TEM and AFM analyses. K.T.S. thanks CSIR-NCL for research fellowship.

■ REFERENCES

- (1) Grimsdale, A. C.; Chan, K. L.; Martin, R. E.; Jokisz, P. G.; Holmes, A. B. *Chem. Rev.* **2009**, *109*, 897–1091.
- (2) Chen, J.; Cao, Y. *Acc. Chem. Res.* **2009**, *42*, 1709–1718.
- (3) Boudreault, P. L. T.; Najari, A.; Leclerc, M. *Chem. Mater.* **2011**, *23*, 456–469.
- (4) Facchetti, A. *Chem. Mater.* **2011**, *23*, 733–758.
- (5) McQuade, D. T.; Pullen, A. E.; Swager, T. M. *Chem. Rev.* **2000**, *100*, 2537–2574.
- (6) Bazan, G. C.; Wang, S. *Springer Ser. Mater. Sci.* **2008**, *107*, 1–37.
- (7) Miranda, O. R.; you, C. C.; Phillips, R.; Kim, I. B.; Ghosh, P. S.; Bunz, U. H. F.; Rotello, V. M. *J. Am. Chem. Soc.* **2007**, *129*, 9856–9857.
- (8) Herland, A.; Inghanas, O. *Macromol. Rapid Commun.* **2007**, *28*, 1703–1713.
- (9) Thomas, S. W., III; Joly, G. D.; Swager, T. M. *Chem. Rev.* **2007**, *107*, 1339–1386.
- (10) Zhou, Q.; Swager, T. M. *J. Am. Chem. Soc.* **1995**, *117*, 12593–12602.
- (11) Gaylord, B. S.; Heeger, A. J.; Bazan, G. C. *J. Am. Chem. Soc.* **2003**, *125*, 896–900.
- (12) Pinto, S. M.; Burrows, H. D.; Pereira, M. M.; Fonseca, S. M.; Dias, F. B.; Mallavia, R.; Tapia, M. J. *J. Phys. Chem. B* **2009**, *113*, 16093–16100.
- (13) Kaeser, A.; Fischer, I.; Abbel, R.; Besenius, P.; Dasgupta, D.; Gillisen, M. A. J.; Portale, G.; Stevens, A. L.; Herz, L. M.; Schenning, A. P. H. J. *ACS Nano* **2012**, DOI: 10.1021/nn305477u.
- (14) Discher, D. E.; Eisenberg, A. *Science* **2002**, *297*, 967–973.
- (15) Jianzhong, Du.; O'Reilly, R. K. *Soft Matter* **2009**, *5*, 3544–3561.
- (16) Yao, J. H.; Mya, K. Y.; Shen, L.; He, B. P.; Li, L.; Li, Z. H.; Chen, Z. K.; Li, X.; Loh, K. P. *Macromolecules* **2008**, *41*, 1438–1443.
- (17) Bonnett, R.; Davies, J. E.; Hursthouse, M. B. *Nature* **1976**, *262*, 326–328.
- (18) Fevery, J. *Liver International* **2008**, 592–605.
- (19) Koelman, J.; Roehm, K. H. *Color Atlas of Biochemistry*, 2nd ed.; Thieme: Stuttgart, Germany, and New York, 2005.
- (20) Van den Bergh, A. A. H.; Snapper, J. *Dtsch. Arch. Klin. Med.* **1913**, *110*, 540–561.
- (21) Rand, R. N.; di Pasqua, A. *Clin. Chem.* **1962**, *8*, 570–578.
- (22) Huber, A. H.; Zhu, B.; Kwan, T.; Kampf, J. P.; Hegyi, T.; Kleinfeld, A. M. *Clin. Chem.* **2012**, *58*, 869–876.
- (23) Pramod, P. S.; Takamura, K.; Chaphekar, S.; Balasubramanian, N.; Jayakannan, M. *Biomacromolecules* **2012**, *13*, 3627–3640.
- (24) Cho, S. Y.; Grimsdale, A. C.; Jones, D. J.; Watkins, S. E.; Holmes, A. B. *J. Am. Chem. Soc.* **2007**, *129*, 11910–11911.
- (25) Ranger, M.; Rondeau, D.; Leclerc, M. *Macromolecules* **1997**, *30*, 7686–7691.
- (26) Grell, M.; Bradley, D. D. C.; Inbasekaran, M.; Woo, E. P. *Adv. Mater.* **1997**, *9*, 798–802.
- (27) Teestov, J.; Fox, M. A. *J. Mater. Chem.* **1999**, *9*, 2117–2122.
- (28) Knaapila, M.; Hase, T. P. A.; Torkkeli, M.; Stepanyan, R.; Bouchenoire, L.; Cheun, H.-S.; Winokur, M. J.; Monkman, A. P. *Crys. Growth Des.* **2007**, *7*, 1706–1711.
- (29) Yao, J. H.; Mya, K. Y.; Shen, L.; He, B. P.; Li, L.; Li, Z. H.; Chen, Z.-K.; Li, X.; Loh, K. P. *Macromolecules* **2008**, *41*, 1438–1443.
- (30) Ahlrichs, R.; Bär, M.; Baron, H. P.; Bauernschmitt, R.; Böcker, S.; Ehrig, M.; Eichkorn, K.; Elliott, S.; Furche, F.; Haase, F.; Häser, M.; Horn, H.; Huber, C.; Huniar, U.; Kattannek, M.; Kölmel, C.; Kollwitz, M.; May, K.; Ochsenfeld, C.; Öhm, H.; Schäfer, A.; Schneider, U.; Treutler, O.; von Arnim, M.; Weigend, F.; Weis, P.; Weiss, H. TURBOMOLE (Version 6.2); Universität Karlsruhe: Karlsruhe, Germany, 2000.
- (31) Becke, A. D. *Phys. Rev. A.* **1988**, *38*, 3098–3100.
- (32) Abbel, R.; van der Weegen, R.; Pisula, W.; Surin, M.; Leclère, P.; Lazzaroni, R.; Meijer, E. W.; Schenning, A. P. H. J. *Chem.—Eur. J.* **2009**, *15*, 9737–9746.
- (33) Stevens, A. L.; Kaeser, A.; Schenning, A. P. H. J.; Herz, L. M. *ACS Nano* **2012**, *6*, 4777–4787.
- (34) Knaapila, M.; Evans, R. C.; Gutacker, A.; Garamus, V. M.; Torkkeli, M.; Adamczyk, S.; Forster, M.; Scherf, U.; Burrows, H. D. *Langmuir* **2010**, *26*, 5056–5066.
- (35) Hotz, J.; Meier, W. *Langmuir* **1998**, *14*, 1031–1036.
- (36) Houga, C.; Giermanska, J.; Lecommandoux, S.; Borsali, R.; Taton, D.; Gnanou, Y.; Francois Le Meins, J. *Biomacromolecules* **2009**, *10*, 32–40.
- (37) Lee, J.; Cho, H. J.; Jung, B. J.; Cho, N. S.; Shim, H. K. *Macromolecules* **2004**, *37*, 8523–8529.
- (38) Li, Y.; Vamvounis, G.; Holdcroft, S. *Macromolecules* **2002**, *35*, 6900–6906.
- (39) Rodes, J.; Benhamou, J.-P.; Blei, A.; Reichen, J.; Rizzetto, M. *The Textbook of Hepatology: From Basic Science to Clinical Practice*, 3rd ed.; Oxford: Malden, Massachusetts, 2007; Chapter 2.
- (40) Zietz, B.; Gillbro, T. *J. Phys. Chem. B.* **2007**, *111*, 11997–12003.
- (41) Corry, B.; Jayatilaka, D.; Rigby, P. *Biophys. J.* **2005**, *89*, 3822–3836.
- (42) Baydemir, G.; Andac, M.; Bereli, N.; Say, R.; Denizli, A. *Ind. Eng. Chem. Res.* **2007**, *46*, 2843–2852.
- (43) Scherf, U.; Neher, D. *Polyfluorene*; Springer-Verlag: Berlin and Heidelberg, Germany, 2008.
- (44) Al Attar, H. A.; Monkman, A. P. *Biomacromolecules* **2009**, *10*, 1077–1083.
- (45) Mcdonagh, A. F.; Palma, L. A. *Biochem. J.* **1980**, *189*, 193–208.